Supplementary Information

In-situ construction of 3D TiO_2 photoelectrode with multilevel facet heterojunctions towards the efficient removal of bisphenol A

Yiqiong Hu, [a] Xiaotong Gu, [a] Guohua Zhao,[a,b] Ya-nan Zhang,[*a,b]

a. School of Chemical Science and Engineering, Shanghai Key Lab of Chemical Assessment and Sustainability.

b. Key Laboratory of Yangtze River Water Environment, Tongji University, Shanghai 200092, People's Republic of China.

Email: yananzhang@tongji.edu.cn

Experimental

Reagents and materials

The main reagents utilized in this study, including ethylenediamine tetraacetatic acid disodium (EDTA-2Na, >99.0%), bisphenol A (≥99.5%), hydrofluoric acid (HF, ≥40.0%), hydrochloric acid (HCl, 36.0~38.0%), hydrogen peroxide (H_2O_2≥30.0%), nitric acid (HNO_3, 65.0~68.0%), anhydrous sodium sulfate (Na_2SO_4, >99.0%), anhydrous sodium sulphite (Na_2SO_3, >99.0%) were all provided by Sinopharm (Shanghai, China). Titanium trichloride ($TiCl_3$, 15%~20%), isopropyl alcohol (IPA, ≥99.5%) and ethanol were purchased from Aladdin Co. (Shanghai, China). Titanium foil substrate (80 mesh, 0.1mm in diameter, ≥99.99%) was obtained from Anping Kangwei wire mesh Products Co., Ltd. All reagents were used without further purification.

Synthesis of FH-{111}TiO_2/Ti

As exhibited in Fig. 1a, three-dimensional (3D) FH-TiO_2/Ti photoelectrodes were facilely constructed via a deft method. It could be intuitively seen that the whole preparation process was divided into two successive steps: the in situ synthesis of 1D TiO_2 nanorods with {111} facets on top ({111}TiO_2/Ti NRs), and the following growth of {101} and {111} nanosheets. Primarily, {111}TiO_2/Ti NRs were in situ fabricated by gas etching. After a 30 s pretreatment with the chemical polish solution (V_{H_2O}: V_{HNO_3}: V_{HF}=20:5:1), the obtained Ti mesh (3.5 cm × 4.5 cm) was placed on a 150 mL Teflon hollow cylindrical support, approximately 6 cm apart from the mixed solvent, which consisted of HCl (2.2 mL) , H_2O_2 (450μL) and deionized water (7.6 mL) to react at 200 ^oC for 5 h. The precursor was thoroughly rinsed with deionized water and dried in ambient air at room temperature (named as {111}TiO_2/Ti).

Subsequently, the FH-{111}TiO_2/Ti samples were prepared by the hydrothermal method, whose {111} and {101} nanosheets following grew on the {111}TiO_2/Ti. Briefly, 250 μL HCl and 100 μL (or 200 μL) $TiCl_3$ were dissolved in 30 mL deionized water to obtain mixed solution, which was transferred into a 100 mL Teflon-lined stainless steel autoclave together with the {111}TiO_2/Ti precursor for 4h at 80 ^oC, followed by washing with deionized water and drying. According to the different concentration of $TiCl_3$, these products were named as L-FH-{111}TiO_2/Ti (100 μL) and H-FH-{111}TiO_2/Ti (200 μL), respectively. All of the photoelectrodes ({111}TiO_2/Ti, L-FH-{111}TiO_2/Ti and H-FH-{111}TiO_2/Ti) were subsequently annealed at 450 °C for 120 min in air prior to further studies.

Characterization

The morphology of photoelectrodes was collected via scanning electron microscopy (SEM, Hitachi–S4800) and transmission electron microscopy (TEM, JEM-2100, JEOL). X–ray diffraction (XRD, D8 Advance Bruker) patterns with Cu Kα as the radiation source over the 2θ range of

20−80° and Raman spectra (Renishaw Crop., UK) were recorded to investigate the crystal phase and structures of materials. X-ray photoelectron spectroscopy (XPS, <10^{-8} torrent, Al target, 150 W, AXIS Ultra DLD, Shimazu Kratos) was conducted to test the element composition of the photoelectrodes. Additionally, UV-visible diffuse reflection spectroscopy (DRS) was obtained on an Agilent Carry 5000 spectrophotometer. Photoluminescence spectrophotometer (PL, F-7000, Japan) was used to explore the charge separation efficiency with a 410 nm excitation wavelength. The PL lifetime was characterized by a time-resolved fluorescence spectrometer (HORIBA Fluorolog-3-11).

PEC performance test

The photoelectrochemical (PEC) performance was measured through a CHI 660c electrochemical workstation in a typical three-electrode structure where the FH-{111}TiO_2/Ti, platinum foil and saturated calomel electrode (SCE) served the function of the working electrode, counter electrode and reference electrode, respectively. And the 0.1 M Na_2SO_4 aqueous solution played a role in electrolyte solution. A 150 W LA-410UV-3 lamp (Hayashi, Japan) as the UV-Vis light source was fixed with 1 cm distance from the working electrode during the PEC process.

Photoelectrocatalytic experiments

The PEC degradation activity was carried out in a 50 mL quartz reactor under the irradiation of a 300 W xenon lamp in the wavelength of 320-780 nm (PLS-SXE300, Perfect Light Technology Co. Ltd., Beijing, China). The 45 mL BPA of 5 mg/L including 0.1 M Na_2SO_4 solution as supporting electrolyte was removed at + 0.4 V *vs*. SCE in a certain time interval. The concentrations of BPA during the degradation period were tested by the HPLC (Agilent 1260). The corresponding mobile phase was 35:65 (v/v) water/acetonitrile mixture with the flow rate of 0.8 mL/min. And the wavelength of UV detector was 225nm. Moreover, the determination of total organic carbon (TOC) was performed by TOC analyser (multi N/C 3100, Analytikjena, Germany).

The scavenging experiment was in accordance with the above procedures accompanied by the addition of isopropyl alcohol (IPA), plenty nitrogen (N_2), ethy-lenediamine tetraacetic acid disodiumn (EDTA-2Na) and L-histidine as the quenching agents for ·OH, $O2^{\cdot-}$, h^+, $^1O_2$, respectively, in order to distinguish the contribution of the main active species. With the increase of the dosage of the above quenching agents, the BPA degradation reached saturation at last.

DFT calculations

To further explore the migration mechanism of the photogenerated carriers, the calculations of the electronic structures were carried out in the utilization of the Vienna Ab-initio Simulation Package (VASP) with the frozen-core all-electron projector-augment-wave (PAW) method. The Perdew-Burke-Ernzerhof (PBE) of generalized gradient approximation (GGA) was adopted to describe the exchange and correlation potential. And the cutoff energy for the plane-wave basis

set was adjusted to 450 eV. The gamma k-point sampling of the Brillouin zone was applied for all calculations. DFT+U7 method was employed for the calculations of energy band structure, in which the effective on-site coulomb interaction parameter of 6 eV was applied to the Ti-3d electrons. The vacuum slab models were constructed to investigate the energy band structure of rutile TiO_2 {110}, {101} and {111} facets, above which was a vacuum region of 20 Å, making the decoupling between adjacent systems sure. For the geometry optimization, all of the atoms were allowed to relax.

Table S1. Summary of light harvesting efficiency (η_{abs}), charge separation efficiency (η_{sep}) and injection efficiency (η_{inj}) of photoelectrodes.

Sample	η_{abs}(%)	η_{sep}(%)	η_{inj}(%)
L-FH-{111}TiO_2/Ti	73.11	49.11	70.28
H-FH{111}TiO_2/Ti	51.07	40.12	64.44
{111}TiO_2/Ti	35.78	32.88	33.55

*: Calculation of light harvesting (η_{abs}), charge separation (η_{sep}) and injection efficiency (η_{inj})

η_{abs} is defined as the fraction of photons absorbed per photons impinging on the photoelectrode, which can be calculated using the following equation: $\eta_{abs} = 1 - 10^{-J_{light}}$

where the J_{light} is the photocurrent at different applied bias in a 0.1 M Na_2SO_4 aqueous solution.

η_{sep} is the yield of photogenerated h^+ which have migrated to the semiconductor/electrolyte interfaces, calculated through the equation: $\eta_{sep} = \frac{J_{Na_2SO_3}}{J_{abs}}$

Theoretical maximum photocurrent density (J_{abs}) is the photocurrent density assuming that all absorbed photons is able to be converted into current. And the J_{abs} of rutile TiO_2 is reported as 1.8 mA/ cm^2.

η_{inj} is deemed as the yield of holes involved in oxidation reaction of BPA. The calculation of η_{inj} is as follows: $\eta_{inj} = \frac{J_{Na_2SO_4}}{J_{Na_2SO_3}}$

The widely used Na_2SO_3 is chosen as the hole scavenger.

Table S2. The time-resolved PL electron lifetime, carrier density, ac impedance and photocurrent density of photoelectrodes.

Sample	τ (ns)	Carrier density ($\times10^{21}$ cm^{-3})	R_{ct} (Ω)	Photocurrent density ($\times10^{-4}$ A cm^{-2})
L-FH-{111}TiO_2/Ti	8.50	3.99	166	5.6
H-FH-{111}TiO_2/Ti	5.64	1.02	286	4.6
{111}TiO_2/Ti	2.30	0.24	625	1.9

Table S3. The VBM, CBM, bandgap and effective mass of photoelectrodes.

Facet	VBM (eV)	CBM (eV)	Bandgap (eV)	Effective Mass
{111}	-6.4008	-4.1128	2.2880	0.194 m_0
{101}	-6.7004	-4.1844	2.5160	0.167 m_0
{110}	-7.2594	-4.6950	2.5644	0.222 m_0

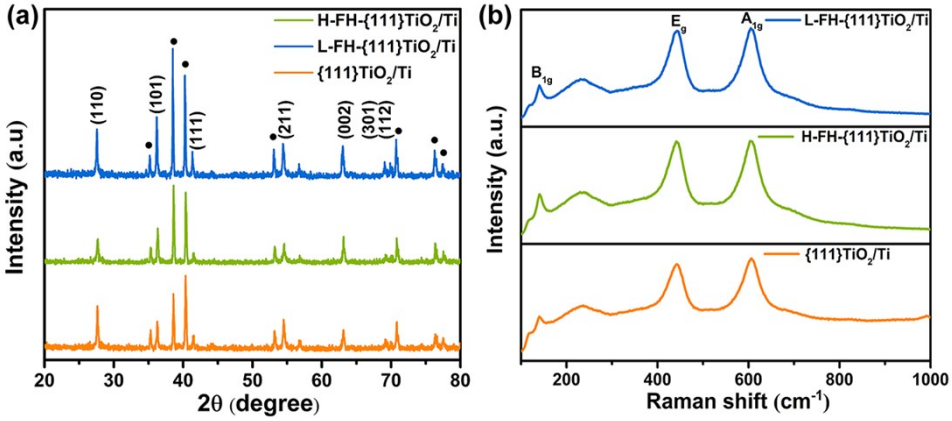

Fig. S1 The XRD (a) and Raman (b) spectrum of photoelectrodes.

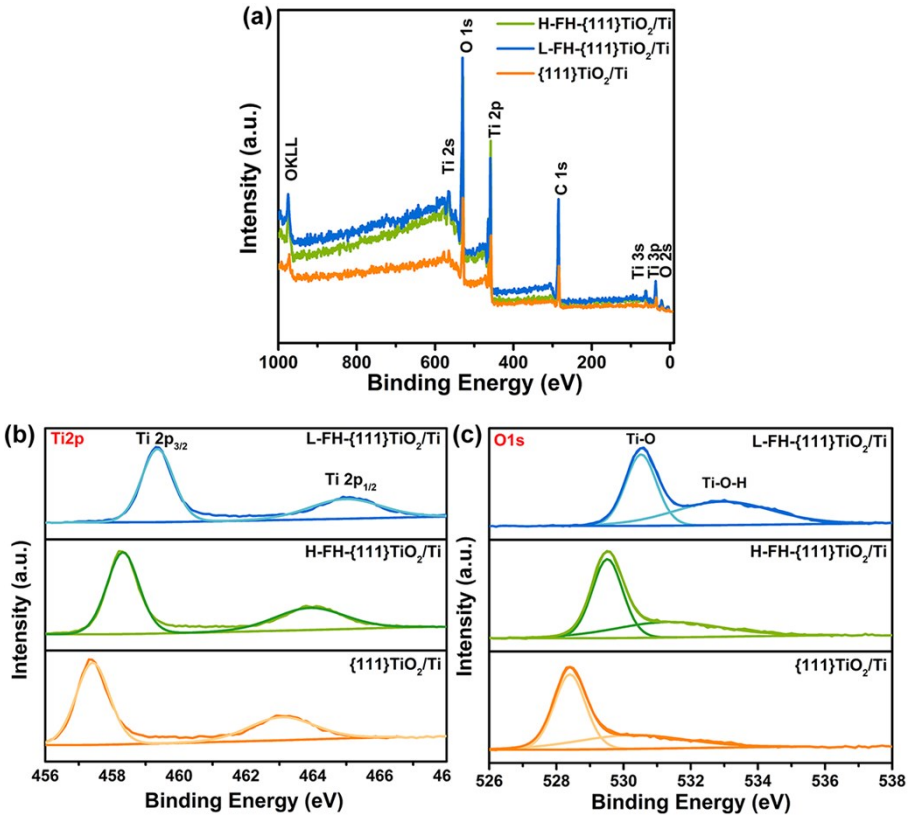

Fig. S2 The XPS spectrum (a) and fine Ti2p (b) and O1S (c) sturcture of photoelectrodes.

The obvious Ti and O elements were probed in wide region X-ray photoelectron spectrum (Fig. S2a). And the distinct peaks at approximately 459.1 and 464.7 eV were confirmed as the Ti $2p_{3/2}$ and Ti $2p_{1/2}$ of Ti^{4+} (Fig. S2b). [18] There were distinctive positive shifts in turn (by 1.0 eV) founded in the Ti 2p binding energy, providing evidence of interactions among {111}, {101} and {110} facets. And two oxygen chemical states could be observed in Fig. S2c approximately at 530.2 and 532.1 eV, assigned to lattice oxygen and hydroxyl oxygen, respectively. [19] The obtained results indicated a decrease in the electron density of TiO_2, accounting for the surface binding interaction between FHs, which boosted an electron transfer.

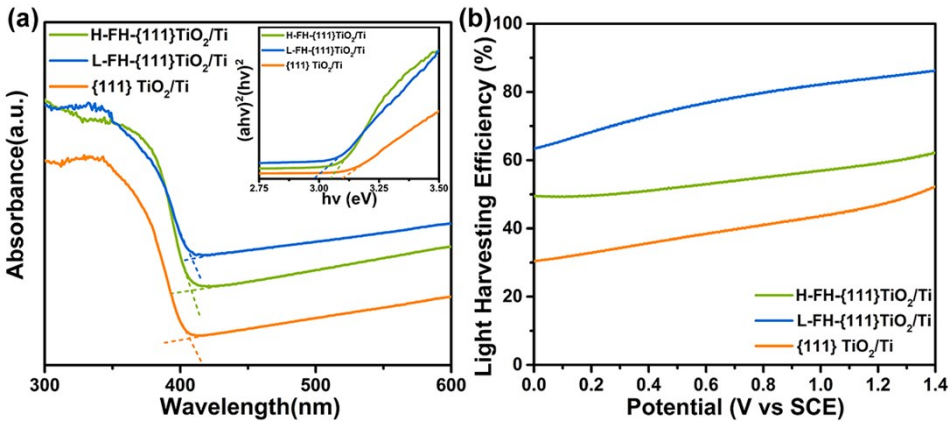

Fig. S3 The UV–vis absorption spectra (a), bandgap (insert) and light harvesting efficiency (η_{abs}) of photoelectrodes.

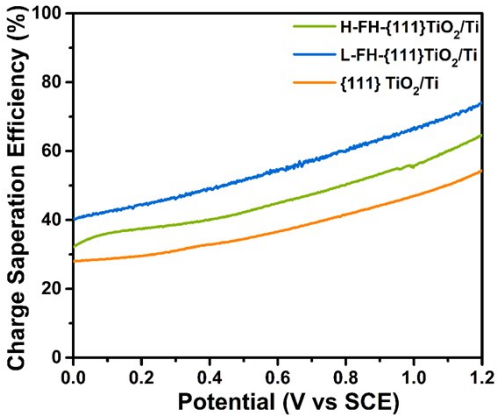

Fig. S4 The charge separation efficiency (η_{sep}) of photoelectrodes.

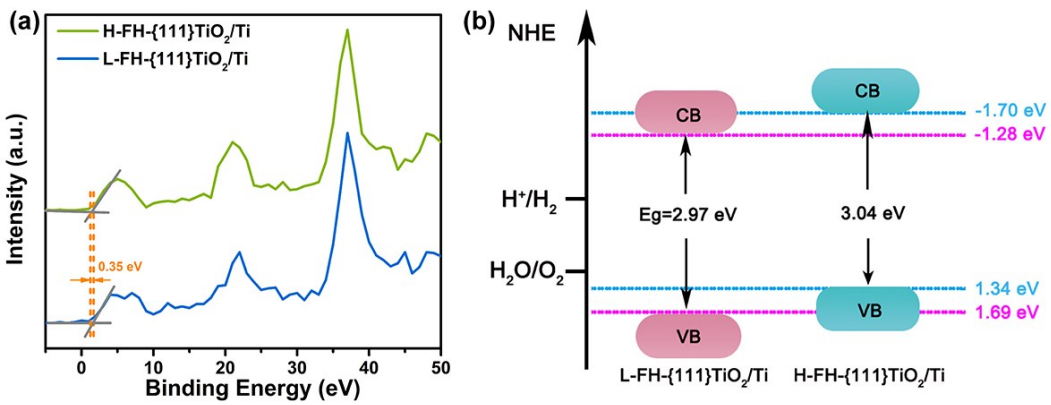

Fig. S5 The valence band spectra (a) and band structure diagrams (b) of FH-{111}TiO_2/Ti photoelectrodes.

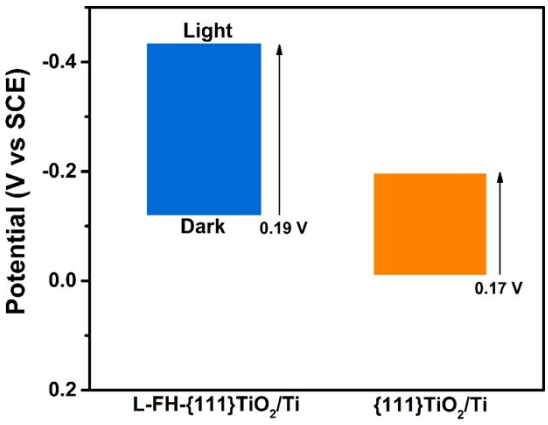

Fig. S6 OCP measurements of L-FH-{111}TiO_2/Ti and {111}TiO_2/Ti.

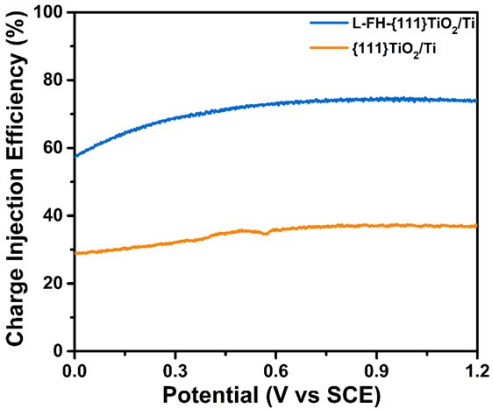

Fig. S7 The charge injection efficiency (η_{inj}) of photoelectrodes.

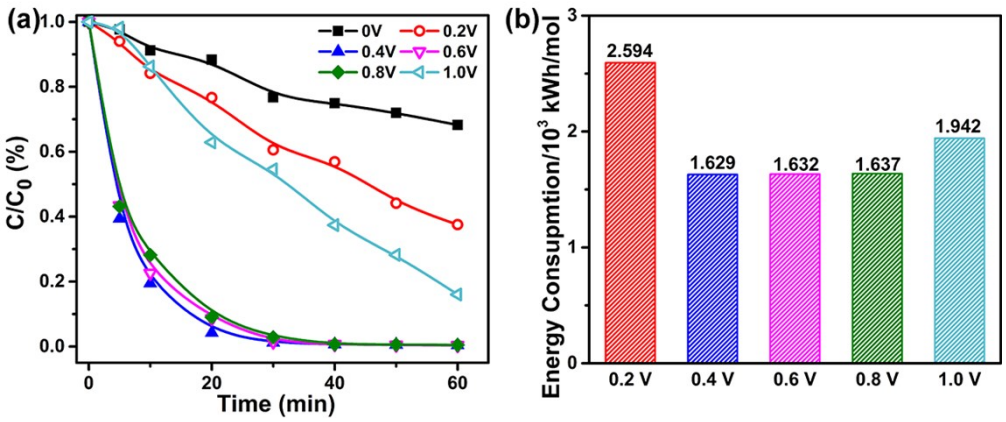

Fig. S8 The PEC degradation rate (a) and energy consumption (b) of BPA by L-FH-{111}TiO_2/Ti under different bias voltages.

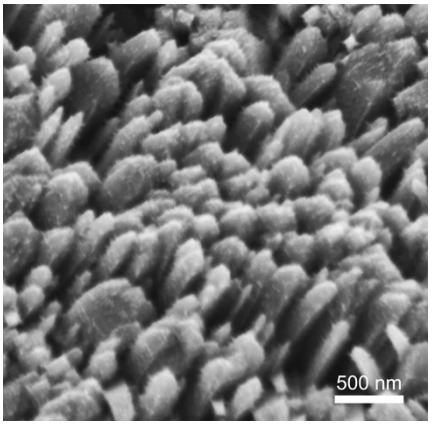

Fig. S9 The SEM images of L-FH-{111}TiO_2/Ti after cycling degradation of BPA.

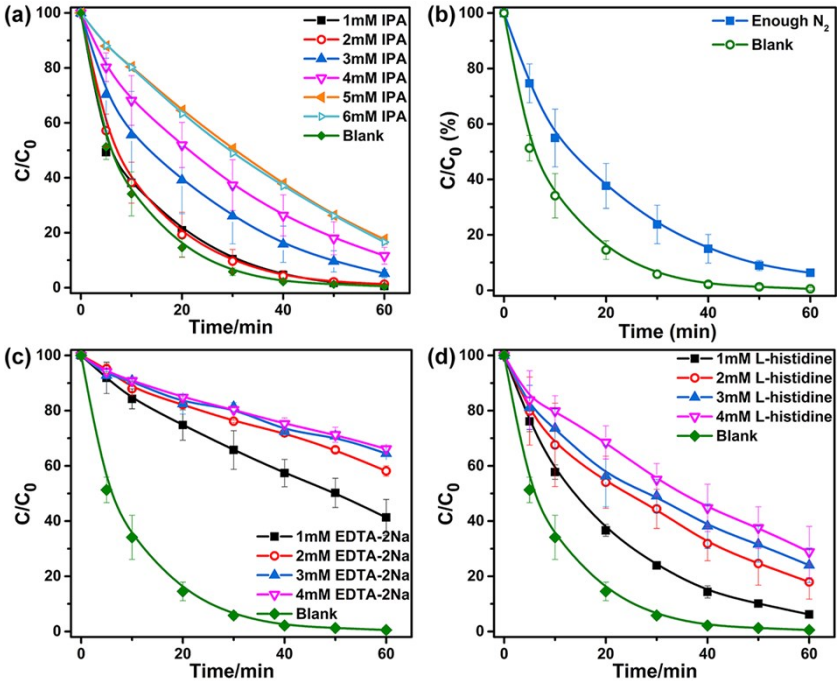

Fig. S10 The PEC degradation rate of BPA with the addition of different scavengers.

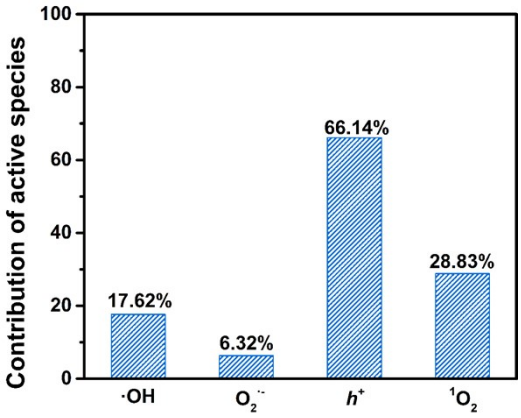

Fig. S11 The contribution of active species to PEC degradation of BPA.